

A Novel Algorithm for Periodic Conformal Flattening of Genus-one and Multiply Connected Genus-zero Surfaces

Zhong-Heng Tan Tiexiang Li Wen-Wei Lin Shing-Tung Yau

Abstract

In this paper, we propose a novel method for genus-one and multiply connected genus-zero surfaces, namely periodic conformal flattening. The primary advantage of this method is its independence from the cut paths and consistency preservation of the cut seams, which introduce no additional conformal distortion near the cut seams. We utilize the conformal energy minimization technique to compute the desired conformal map, which is characterised as an easy-solved quadratic functional minimization problem. The numerical experiments illustrate that our proposed algorithms DPCF and SPCF is of high accuracy and a 4-5 times improvement in terms of efficiency compared with state-of-the-art algorithms.

Key words— periodic conformal flattening, conformal energy minimization, genus-one surface, multiply connected genus-zero surface

1 Introduction

The advent of high-precision 3D technology has given rise to a plethora of surfaces that are characterised by high resolution and complex geometries, which poses challenges to direct surface manipulation. Surface flattening is a fundamental technique that aims to flatten a surface onto a plane, transforming the processing of the complicated surface into that of a simple 2D domain. Generally, the flattening map should be bijective or local injective to ensure optimal visual effects and processing performance in practical applications, which is the focus of some works [10, 28, 29]. The another common goal of the surface flattening is to minimize the flattening distortion. Conformal flattening is a flattening technique minimizing the conformal distortion, which preserves the local shape upon the conformal map. Consequently, it plays a significant role in computer-aided engineering [20, 3] and computer graphics [13, 21].

Various algorithms and methods have been developed to achieve surface conformal flattening, including MIPS [14], angle-based flattening [25, 26], LSCM [21], DCP [7], circle patterns [18], Ricci flow [17, 30], spectral conformal parameterization [23], discrete conformal equivalence [11]. Recently, Rohan Sawhney and Keenan Crane utilized Yamabe equation [24] to flatten the surface with various boundary conditions. The Yamabe equation describes the relation between the conformal factor and Gauss curvature, which is an intrinsic approach for the surface flattening. [6, 5, 4] developed quasi-conformal map methods, which uses the composition of several quasi-conformal maps to achieve the conformal map. Additionally, conformal energy minimization is proposed for disk parameterizations [32, 19] and free boundary flattening [15].

Notably, the surface flattening is a topology-preserving process, i.e., the surface and the flattened domain are topologically equivalent. Therefore, for the surfaces such as sphere and torus, a cutting procedure making the surface be able to be flattened should be applied before the flattening. The two edges at the cut seam are the identical after cutting. For such a cut surface, conventional surface flattening techniques often result in a bias near the cut path and complex correspondence between the two cut edges, which hinders the efficacy of practical applications such as texture mapping and mesh generation. Choi [4] computed the annulus conformal parameterizations by firstly cutting the surface into disk-topology and then transform it into a rectangle by a quasi-conformal map. The cut path is restricted to be a straight line during the rectangle transformation procedure, and finally the composition of quasi-conformal maps is utilized to mitigate the conformal distortion near the cut

seam, which, however, is not completely eliminated. To address this challenge, the seamless parameterization [1, 27, 9] has been proposed, which, intuitively, introduces constraints that restrict the simple correspondence of the edges at the cut seam, thereby ensuring that the parameterization distortion remains independent to the cut path selection. Noam Aigerman et al proposed G-flattening [1] for computing seamless bijective mappings between two meshes, implicitly restricting the correspondence to be translation, scaling and rotation, while the resulting map is not conformal. Rotationally seamless parameterizations [2, 22] were developed for quadrilateral mesh generation and texture mapping, which restricts that the rotational angle between the cut path must be the multiple of $\pi/2$.

Different to seamless parameterization, in this paper, we aim to compute conformal flattening with correspondence of the cut path to be only translation for the conformal parameterization of genus-one surface and multiply connected genus-zero surface via conformal energy minimization. Since the flattening with only translation for genus-one and doubly connected surfaces leads to a periodic tiling on \mathbb{R}^2 , we call it ‘periodic conformal flattening’. The main contribution of this paper is threefold.

- We introduce periodicity in conformal flattening of genus-one and multiply connected genus-zero surfaces based on the previously proposed seamlessness property, which eliminate the inconsistency occurring at cut seams. Under the periodic conformal flattening, the computed conformal map is independent of the cut seam selection and no additional conformal distortions occur at the cut seam.
- We utilize the conformal energy minimization to compute the periodic conformal flattening. Since the target domain of the conformal map is a polygon, the conformal energy can be represented as a quadratic functional with respect to the vertices and period. Thus, conformal energy minimization becomes a linear system solution problem, which makes our proposed algorithms DPCF and SPCF very efficient. Meanwhile, the linear system automatically calculates the optimal translation vectors and, for genus-one surfaces, the angle between the translation vectors of the two periods is automatically adjusted to minimize the conformal distortions.
- Numerical experiments and comparisons with existing algorithms demonstrate the advantages of both DPCF and SPCF in terms of efficiency and accuracy. For the genus-one surface, our proposed DPCF has almost identical conformal accuracy with holomorphic approach [31] and 4-5 times of efficiency. For the multiply connected surface, our proposed SPCF has better conformality and improves 3-4 times of efficiency compared with ACM (PACM) [4]. On the other hand, there is no additional distortion near the cut path according to the angle distortion distributions, illustrating the independence of our algorithms to the cut path selection.

This paper is organized as follows. In Section 2, we briefly introduce the discrete surface and review the conformal energy. In Section 3, we derive the conformal energy minimization for double periodic conformal flattening on genus-one surfaces. In Section 4, we derive the conformal energy minimization for single periodic conformal flattening and its applications on annulus and poly-annulus parameterizations. The numerical performance and comparison with holomorphic approach [31] and ACM (PACM) [4] are presented in Section 5. A concluding mark is given in Section 6.

The frequently used notations in this paper are listed here. Bold letters, e.g., \mathbf{a}, \mathbf{s} , denote vectors. $\mathbf{1}_{m \times n}$ denotes the $m \times n$ matrix of all ones. The notation without the subscript $\mathbf{1}$ denotes the vector of all ones with the appropriate dimension. e_i denotes the i -th column of the identity matrix with the appropriate dimension. $[A]_{ij}$ denotes the (i, j) -th entry of matrix A . $\text{diag}(\mathbf{a})$ denotes the diagonal matrix with the (i, i) -th entry being \mathbf{a}_i .

2 Discrete Surface and Conformal Energy

In this section, we briefly introduce discrete surfaces and review the conformal energy. Let \mathcal{M} be a discrete surface, which consists of the sets of vertices

$$\mathcal{V}(\mathcal{M}) = \{v_s = (v_s^1, v_s^2, v_s^3) \in \mathbb{R}^3\}_{s=1}^n, \quad (2.1)$$

faces

$$\mathcal{F}(\mathcal{M}) = \{[v_i, v_j, v_k] \subset \mathbb{R}^3 \mid \text{for some } \{v_i, v_j, v_k\} \subset \mathcal{V}(\mathcal{M})\}, \quad (2.2)$$

where the bracket $[v_i, v_j, v_k]$ denotes a triangle, i.e., the convex hull of the affinely independent vertices $\{v_i, v_j, v_k\}$, and edges

$$\mathcal{E}(\mathcal{M}) = \{[v_i, v_j] \subset \mathbb{R}^3 \mid \{v_i, v_j, v_k\} \in \mathcal{F}(\mathcal{M}) \text{ for some } v_k \in \mathcal{V}(\mathcal{M})\}. \quad (2.3)$$

The discrete map f defined on the discrete surface \mathcal{M} is considered to be piecewise affine. Under this view, the image location $f(v)$ for a point v in a triangle $[v_i, v_j, v_k] \subset \mathcal{M}$ can be represented by barycentric coordinates

$$f(v) = \frac{[v, v_j, v_k]}{[v_i, v_j, v_k]} f(v_i) + \frac{[v_i, v, v_k]}{[v_i, v_j, v_k]} f(v_j) + \frac{[v_i, v_j, v]}{[v_i, v_j, v_k]} f(v_k). \quad (2.4)$$

Let $\mathbf{f}_\ell = f(v_\ell)$ for $\ell = 1, 2, \dots, n$ and define the image vertices matrix $\mathbf{f} := [\mathbf{f}_1^T, \mathbf{f}_2^T, \dots, \mathbf{f}_n^T]^T$. The map f is induced by \mathbf{f} via the barycentric coordinates in (2.4).

The continuous conformal energy functional [16] for a map f defined on \mathcal{M} is defined as

$$E_C(f) = \frac{1}{2} \int_{\mathcal{M}} \|\nabla_{\mathcal{M}} f\|_F^2 ds - |f(\mathcal{M})|, \quad (2.5)$$

where $\nabla_{\mathcal{M}}$ represents the tangent gradient and $|f(\mathcal{M})|$ is the area of the image surface $f(\mathcal{M})$. The conformal energy satisfies that $E_C(f) \geq 0$ for arbitrary map f and $E_C(f) = 0$ if and only if f is conformal. Therefore, the conformal map can be computed by minimizing the conformal energy.

Numerically, the discrete conformal energy for a piecewise affine map f defined on the discrete surface \mathcal{M} becomes

$$E_C(f) = \frac{1}{2} \text{trace}(\mathbf{f}^T L_D \mathbf{f}) - |f(\mathcal{M})|, \quad (2.6)$$

where L_D is the Laplacian matrix with

$$[L_D]_{ij} = \begin{cases} -w_{ij} \equiv -\frac{1}{2}(\cot \theta_{ij} + \cot \theta_{ji}), & \text{if } [v_i, v_j] \in \mathcal{E}(\mathcal{M}), \\ \sum_{\ell \neq i} w_{i\ell}, & \text{if } i = j, \\ 0, & \text{otherwise,} \end{cases} \quad (2.7)$$

in which θ_{ij} and θ_{ji} are the opposite angles of edge $[v_i, v_j]$, as shown in Figure 1.

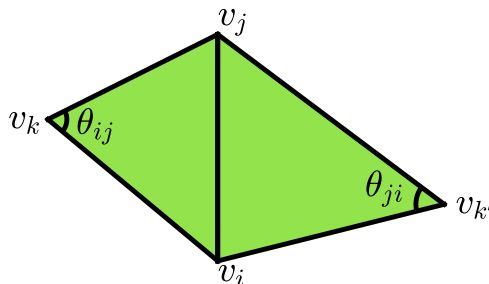


Figure 1: The opposite angles of edge $[v_i, v_j]$.

3 Double Periodic Conformal Flattening of Genus-One Surfaces

Let \mathcal{M} be a genus-one surface. We first illustrate the uniformization theorem [12] for the classification of simply connected Riemann surface upon the conformal map.

Theorem 1 (Poincaré-Klein-Koebe Uniformization [12]). *A simply connected Riemann surface is conformally equivalent to one of the following three canonical Riemann surface:*

1. *Extended complex plane $\overline{\mathbb{C}} = \mathbb{C} \cup \{\infty\}$;*
2. *Complex plane \mathbb{C} ;*
3. *Open unit disk $\Delta = \{z \in \mathbb{C} \mid |z| < 1\}$.*

The mentioned three types of surfaces corresponds to the simply connected Riemann surfaces with genus = 0, genus = 1 and genus > 1, respectively. Furthermore, the genus-one surface \mathcal{M} is conformally equivalent to a quotient group \mathbb{C}/G , where G is the deck transformation group

$$G = \{z \rightarrow z + k_1 w_1 + k_2 w_2, k_1, k_2 \in \mathbb{Z}, w_1, w_2 \in \mathbb{C}, \text{Im}(w_1/w_2) \neq 0\}. \quad (3.1)$$

This means that a genus-one surface can be conformally transformed into the unit cell of a 2D lattice

$$\Lambda_{h,t} = \{k_1 h + k_2 t, k_1, k_2 \in \mathbb{Z}, h, t \in \mathbb{R}^{1 \times 2}, \det([h^T, t^T]) \neq 0\}. \quad (3.2)$$

Geometrically, there exists a homeomorphism that transforms \mathcal{M} into a domain \mathcal{T} with doubly periodic boundary. This domain \mathcal{T} , as a unit cell, can be used to tile the entire 2D plane \mathbb{R}^2 by translating along the lattice $\Lambda_{h,t}$, as illustrated in Figure 2. In the unit cell \mathcal{T} , the blue and red lines correspond to the handle and tunnel loops, respectively, which form the homology basis of a torus. Our goal is to find a conformal map to transform \mathcal{M} into the unit cell domain \mathcal{T} . Since the unit cell has two pairs of periodic boundaries, this approach is called **Double Periodic Conformal Flattening (DPCF)**.

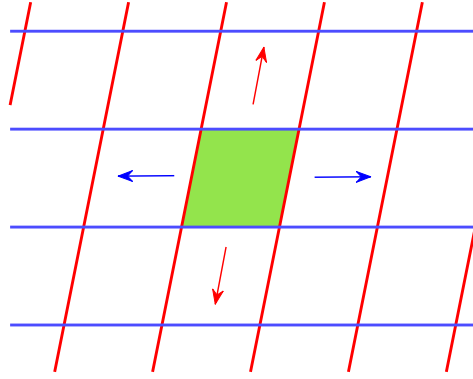


Figure 2: A 2D lattice and the unit cell domain with doubly periodic boundary.

In the discrete version, let \mathcal{M} be a discrete genus-one surface with a handle loop

$$\alpha = \{[a_0, a_1], [a_1, a_2], \dots, [a_{h-1}, a_h], [a_h, a_0]\} \subset \mathbb{R}^3, \quad (3.3a)$$

and a tunnel loop

$$\beta = \{[b_0, b_1], [b_1, b_2], \dots, [b_{t-1}, b_t], [b_t, b_0]\} \subset \mathbb{R}^3, \quad (3.3b)$$

where $a_0 = b_0$, α and β have no self-intersection, but only intersect at a_0 , as shown in Figure 3a. We first cut the mesh of \mathcal{M} along α and β , respectively, to get a new mesh with

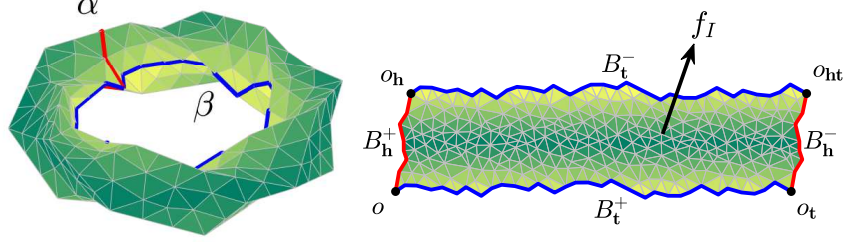
$$\widetilde{\mathcal{M}} = \mathcal{M} \setminus (\alpha \cup \beta) \cup \partial \widetilde{\mathcal{M}}, \quad \partial \widetilde{\mathcal{M}} = \alpha^+ \cup \alpha^- \cup \beta^+ \cup \beta^-. \quad (3.4)$$

Let $\widetilde{\mathcal{T}}$ be a double periodic domain with four vertices $\{O = (0, 0), O_h = (h^1, h^2), O_t = (t^1, t^2), O_{ht} = (h^1 + t^1, h^2 + t^2)\}$ and four sides $\{\overline{OO_h}, \overline{O_h O_{ht}}, \overline{O_{ht} O_t}, \overline{O_t O}\}$ to be determined, as in Figure 3b, in which f_I denotes the interior vertices of $\widetilde{\mathcal{T}}$, B_h^\pm , B_t^\pm denote the vertices of line segments $\overline{OO_h}$, $\overline{O_h O_{ht}}$, $\overline{O_{ht} O_t}$ and $\overline{O_t O}$, respectively. Let \mathcal{T} be a unit cell of $\Lambda_{h,t}$ associated with $\widetilde{\mathcal{T}}$ satisfying identical conditions

$$\overline{OO_h} = \overline{O_{ht} O_t}, \quad \overline{O_h O_{ht}} = \overline{O_t O}. \quad (3.5)$$

Let \mathcal{M} be a discrete genus-one surface and $\widetilde{\mathcal{M}}$ be the slicing surface of \mathcal{M} as in (3.3) along the loops α and β . Based on the Poincaré-Klein-Koebe uniformization theorem, for a given genus-one surface \mathcal{M} , we will find a conformal parameterization

$$f : \mathcal{M} \rightarrow \mathcal{T} \quad (3.6a)$$



(a) Genus-one surface with handle loop α and tunnel loop β (b) Flattened double periodic domain $\tilde{\mathcal{T}}$

Figure 3: An illustrative example of double periodic conformal flattening.

with

$$f := [f^1, f^2] = [f_I^T, (B_t^+)^T, (B_h^+)^T, O^T]^T \in \mathbb{R}^{n \times 2}. \quad (3.6b)$$

We now design a practical novel algorithm to find f in (3.6). We extend f to \tilde{f} from $\tilde{\mathcal{M}}$ to $\tilde{\mathcal{T}}$ with identical conditions of (3.4) by

$$\tilde{f}: \tilde{\mathcal{M}} \rightarrow \tilde{\mathcal{T}}, \quad (3.7a)$$

with

$$\tilde{f} = \begin{bmatrix} f_I \\ B_t^+ \\ B_h^+ \\ O \\ B_t^- \\ B_h^- \\ O_h \\ O_t \\ O_{ht} \end{bmatrix} = \left[\begin{array}{ccc|ccc} I & & & & & \\ & I & & & & \\ & & I & & & \\ & & & 1 & & \\ \hline & & & & I & \\ & & & & & \mathbf{1} \\ & & & & & & \mathbf{1} & 0 \\ & & & & & & & \mathbf{1} \\ & & & & & & & & \mathbf{1} & 1 \\ & & & & & & & & & & \mathbf{1} & 1 & 1 \end{array} \right] \begin{bmatrix} f_I \\ B_t^+ \\ B_h^+ \\ O \\ h \\ t \end{bmatrix} := P \begin{bmatrix} f \\ h \\ t \end{bmatrix} \equiv Pg. \quad (3.7b)$$

The original conformal energy minimization (CEM) algorithm for the computation of the conformal parameterization from a genus-one surface \mathcal{M} to a torus T is to minimize the discrete conformal energy functional as in (2.6). We now define the cutting Laplacian matrix for $\tilde{\mathcal{M}}$ as in (3.4) with

$$[\tilde{L}_D]_{ij} = \begin{cases} -w_{ij} \equiv -\frac{1}{2}(\cot \theta_{ij} + \cot \theta_{ji}), & \text{if } [v_i, v_j] \notin \mathcal{E}(\partial \tilde{\mathcal{M}}), \\ -w_{ij} \equiv -\frac{1}{2} \cot \theta_{ij}, & \text{if } [v_i, v_j] \in \mathcal{E}(\partial \tilde{\mathcal{M}}), \\ \sum_{\ell \neq i} w_{i\ell}, & \text{if } i = j, \\ 0, & \text{otherwise,} \end{cases} \quad (3.8)$$

and consider minimizing the slicing discrete conformal energy functional

$$E_C(\tilde{f}) = E_D(\tilde{f}) - A(\tilde{f}) = \frac{1}{2} \text{trace}(\tilde{f}^T \tilde{L}_D \tilde{f}) - (t^1 h^2 - t^2 h^1). \quad (3.9)$$

From (3.6) and (3.7), the slicing conformal energy in (3.9) can be written as

$$E_C(g) = E_C(f, h, t) = \frac{1}{2} \text{trace}(g^T P^T \tilde{L}_D P g) - |\tilde{\mathcal{T}}| \quad (3.10)$$

$$= \frac{1}{2} \text{trace}(g^T L g) - (t^1 h^2 - t^2 h^1). \quad (3.11)$$

where

$$L := P^T \tilde{L}_D P = \begin{bmatrix} L_D & S \\ S^T & K \end{bmatrix}, \quad K = \begin{bmatrix} k_{11} & k_{12} \\ k_{12} & k_{22} \end{bmatrix} \text{ symmetric}, \quad (3.12)$$

$S = [s_1, s_2]$ with $\mathbf{1}^\top s_j = 0$, $j = 1, 2$, and L_D is the Laplacian matrix corresponding to vertices on \mathcal{M} .

Write $g = [g^1, g^2]$, $f = [f^1, f^2]$ and map f from $(a_0 = b_0)$ in (3.3) to $O = (0, 0)$. The partial derivative of $E_C(g)$ with respect to $\text{vec}(g)$ is

$$\frac{\partial E_C(g)}{\partial \text{vec}(g)} = \begin{bmatrix} Lg^1 \\ Lg^2 \end{bmatrix} - \begin{bmatrix} \mathbf{0} \\ t^2 \\ -h^2 \\ \mathbf{0} \\ -t^1 \\ h^1 \end{bmatrix} \quad (3.13)$$

$$= \frac{\begin{bmatrix} L_D f^1 + s_1 h^1 + s_2 t^1 \\ \begin{bmatrix} s_1^\top \\ s_2^\top \end{bmatrix} f^1 + K \begin{bmatrix} h^1 \\ t^1 \end{bmatrix} - \begin{bmatrix} t^2 \\ -h^2 \end{bmatrix} \\ L_D f^2 + s_1 h^2 + s_2 t^2 \\ \begin{bmatrix} s_1^\top \\ s_2^\top \end{bmatrix} f^2 + K \begin{bmatrix} h^2 \\ t^2 \end{bmatrix} - \begin{bmatrix} -t^1 \\ h^1 \end{bmatrix} \end{bmatrix}}{\begin{bmatrix} L_D f^1 + s_1 h^1 + s_2 t^1 \\ \begin{bmatrix} s_1^\top \\ s_2^\top \end{bmatrix} f^1 + K \begin{bmatrix} h^1 \\ t^1 \end{bmatrix} - \begin{bmatrix} t^2 \\ -h^2 \end{bmatrix} \\ L_D f^2 + s_1 h^2 + s_2 t^2 \\ \begin{bmatrix} s_1^\top \\ s_2^\top \end{bmatrix} f^2 + K \begin{bmatrix} h^2 \\ t^2 \end{bmatrix} - \begin{bmatrix} -t^1 \\ h^1 \end{bmatrix} \end{bmatrix}} = 0. \quad (3.14)$$

From (3.6), we let

$$\hat{L}_0 = L_D(1 : \text{end} - 1, 1 : \text{end} - 1), \quad (3.15a)$$

$$\hat{f} \equiv [\hat{f}^1, \hat{f}^2] = \begin{bmatrix} f_I \\ B_t^+ \\ B_h^+ \end{bmatrix}. \quad (3.15b)$$

Then (3.14) becomes the following two linear systems

$$\begin{bmatrix} \hat{L}_0 & s_1 \\ s_1^\top & k_{11} \end{bmatrix} \begin{bmatrix} \hat{f}^1 \\ h^1 \end{bmatrix} = \begin{bmatrix} -t^1 s_2 \\ -k_{12} t^1 + t^2 \end{bmatrix}, \quad (3.16a)$$

$$\begin{bmatrix} \hat{L}_0 & s_1 \\ s_1^\top & k_{11} \end{bmatrix} \begin{bmatrix} \hat{f}^2 \\ h^2 \end{bmatrix} = \begin{bmatrix} -t^2 s_2 \\ -k_{12} t^2 - t^1 \end{bmatrix}. \quad (3.16b)$$

In practice, we set $t = (t^1, t^2) = (1, 0)$ to be well-known. Then the linear systems (3.16) can be solved for the desired conformal parameterization,

$$\tilde{f} = [f_I^\top, (B_t^+)^{\top}, (B_h^+)^{\top}, O^\top, (B_t^-)^{\top}, (B_h^-)^{\top}, O_h^\top, O_t^\top, O_{ht}^{\top}]^\top, \quad (3.17a)$$

from $\tilde{\mathcal{M}}$ to $\tilde{\mathcal{T}}$, for which

$$B_t^- = B_t^+ + (h^1, h^2), \quad B_h^- = B_h^+ + (t^1, t^2), \quad (3.17b)$$

$$O_t = (t^1, t^2), \quad O_h = (h^1, h^2), \quad O_{ht} = (h^1 + t^1, h^2 + t^2). \quad (3.17c)$$

Remark 1. Since the Poincaré-Klein-Koebe uniformization theorem does not state the relationship of w_1 and w_2 , we do not restrain $h \perp t$ in the practical computation, but automatically compute the best relationship between h and t by CEM instead. In fact, the relationship of h and t depends on the surface itself and the loops to be selected.

4 Single Periodic Conformal Flattening for Multiply Connected Surfaces

Now, we turn to the Single Periodic Conformal Flattening (SPCF) for doubly connected surfaces, which release an identical condition of two boundaries compared with the double periodic conformal flattening. As in Figure 4, doubly connected surface is conformally equivalent to the unit cell of a 1D lattice with two boundaries on \mathbb{R}^2

$$\Lambda_t = \{kt, k \in \mathbb{Z}, t \in \mathbb{R}^{1 \times 2}\}. \quad (4.1)$$



Figure 4: A 1D lattice with two boundaries and the unit cell domain with single periodic boundary.

Therefore, we aim to find a conformal map from the doubly connected surface to a single periodic domain.

Let \mathcal{M} be a discrete doubly connected surface with β_I and β_O being inner and outer boundaries, respectively, in which α^+ and α^- are the left and right slicing curves, respectively, of the cutting curve α on \mathcal{M} . We have the surface $\widetilde{\mathcal{M}} = (\mathcal{M} \setminus \alpha) \cup (\alpha^+ \cup \alpha^-)$, as in Figure 5a. Let \widetilde{R} be a single periodic domain with four vertices $\{O = (0, 0), O_t = (t^1, t^2), O_h = (h^1, h^2), O_{ht} = (h^1 + t^1, h^2 + t^2)\}$, $f_I, B_O, B_I, B_C^- = B_C^+ + t$ being the corresponding interior points of $\widetilde{\mathcal{M}} \setminus (\beta_O \cup \beta_I \cup \alpha^\pm)$, $\beta_O \setminus \{O, O_t\}$, $\beta_I \setminus \{O_h, O_{ht}\}$ and $B_C^+ \setminus \{O, O_h\}$, respectively.

For a given discrete doubly connected surface \mathcal{M} , we will find a conformal parameterization

$$\widetilde{f} : \widetilde{\mathcal{M}} \rightarrow \widetilde{R} \quad (4.2a)$$

with

$$\widetilde{f} = [\widetilde{f}^1, \widetilde{f}^2] = [f^T, |(B_C^-)^T, O_h^T, O_t^T, O_{ht}^T|^T], \quad (4.2b)$$

$$f = [f^1, f^2] = [f_I^T, B_O^T, B_I^T, (B_C^+)^T, O^T]^T, \quad (4.2c)$$

satisfying

$$\widetilde{f} = \begin{bmatrix} f_I \\ B_O \\ B_I \\ B_C^+ \\ O \\ B_C^- \\ O_h \\ O_t \\ O_{ht} \end{bmatrix} = \left[\begin{array}{ccc|cc} I & & & & \\ & I & & & \\ & & I & & \\ & & & 1 & \\ \hline & & & I & 0 & 1 \\ & & & & 1 & 0 \\ & & & & 1 & 0 & 1 \\ & & & & 1 & 1 & 1 \end{array} \right] \begin{bmatrix} f_I \\ B_O \\ B_I \\ B_C^+ \\ O \\ \hline h \\ t \end{bmatrix} := Pg. \quad (4.3)$$

As in (3.9), we consider minimizing the slicing discrete energy functional

$$E_C(\widetilde{f}) = E_D(\widetilde{f}) - A(\widetilde{f}) = \frac{1}{2} \text{trace}(\widetilde{f}^T \widetilde{L}_D \widetilde{f}) - |\widetilde{R}|. \quad (4.4)$$

where \widetilde{L}_D is defined as in (3.8). We abuse the notations in (3.12) and let

$$L := P^T \widetilde{L}_D P = \begin{bmatrix} L_D & S \\ S^T & K \end{bmatrix}, \quad K = \begin{bmatrix} k_{11} & k_{12} \\ k_{12} & k_{22} \end{bmatrix} \text{ symmetric}, \quad (4.5)$$

Additionally, by Gauss's area formula, $|\tilde{R}|$ can be represented by

$$|\tilde{R}| = \frac{1}{2}(\tilde{f}^1)^\top \left[\begin{array}{ccc|cc} \mathbf{0} & & & & & \\ & D_O & & -e_1 & & e_{n_O} \\ & & D_I & & & e_{n_I} \\ & & & \mathbf{0} & & -e_1 \\ e_1^\top & & & 0 & -1 & \\ \hline & & & & \mathbf{0} & \\ & & -e_{n_I}^\top & 1 & 0 & \\ -e_{n_O}^\top & & & & & 0 \\ & & e_1^\top & & & -1 \\ & & & & & 0 \end{array} \right] \tilde{f}^2 \quad (4.6)$$

$$= \frac{1}{2}(g^1)^\top \left[\begin{array}{ccc|cc} \mathbf{0} & & & & & \\ & D_O & & e_{n_O} - e_{1_O} & & e_{n_O} \\ & & D_I & e_{n_I} - e_{1_I} & e_{n_I} - e_{1_I} & -e_{1_I} \\ & & & \mathbf{0} & & 0 \\ e_{1_O}^\top - e_{n_O}^\top & e_{1_I}^\top - e_{n_I}^\top & & 0 & & \\ \hline & & & & 0 & -1 \\ & & -e_{n_O}^\top & e_{1_O}^\top & & 1 \\ & & & & & 0 \end{array} \right] g^2 \equiv (g^1)^\top D g^2, \quad (4.7)$$

in which

$$D_O = \begin{bmatrix} 0 & 1 & & & & \\ -1 & 0 & 1 & & & \\ & & -1 & 0 & \ddots & \\ & & & \ddots & \ddots & \\ & & & & & 0 & 1 \\ & & & & & -1 & 0 \end{bmatrix}, \quad e_{1_O} = \begin{bmatrix} 1 \\ 0 \\ 0 \\ \vdots \\ 0 \end{bmatrix}, \quad e_{n_O} = \begin{bmatrix} 0 \\ 0 \\ \vdots \\ 0 \\ 1 \end{bmatrix}, \quad (4.8)$$

and so are D_I, e_{1_I}, e_{n_I} except the sizes. Substituting (4.5) and (4.7) into (4.4), we have

$$E_C(g) = \frac{1}{2} \text{trace}(g^\top A g), \quad A = \begin{bmatrix} L & -D \\ D & L \end{bmatrix}. \quad (4.9)$$

4.1 Annulus conformal parameterizations

An analytic conformal map from a rectangle $[0, L] \times [0, 1]$ with L to an annulus with inner radius $\exp(-2\pi L^{-1})$ and outer radius 1 is

$$\Pi(x, y) = e^{2\pi(y-L^{-1})} (\cos(2\pi x), \sin(2\pi x)). \quad (4.10)$$

Observing that (4.10) is periodic along the x -direction, the conformality also holds for the x -periodic domain with base L and height 1. Therefore, we can compute the conformal periodic map f by minimizing (4.9) with vertices B_O on line $y = 0$ and B_I on line $y = 1$, and then impose Π on the parameterized domain. The composite map $h := \Pi \circ f$ is the annulus conformal parameterization. We conclude this approach in Algorithm 1.

This approach avoids the circular constrains on the boundaries and adopts two-step conformal maps by only solving a linear system instead. Compared with the solving CEM subject to the circular constrains, there only introduces the additional discrete error of (4.10).

4.2 Poly-Annulus conformal parameterizations

We now consider a multiply connected genus-zero surface \mathcal{M} , i.e., a genus-zero surface with multiple boundaries $\{\beta_\ell, \ell = 1, 2, \dots, N\}$, where β_N is the outer boundary, i.e.

$$\partial\mathcal{M} = \beta_N - \beta_1 - \beta_2 - \dots - \beta_{N-1}, \quad (4.11)$$

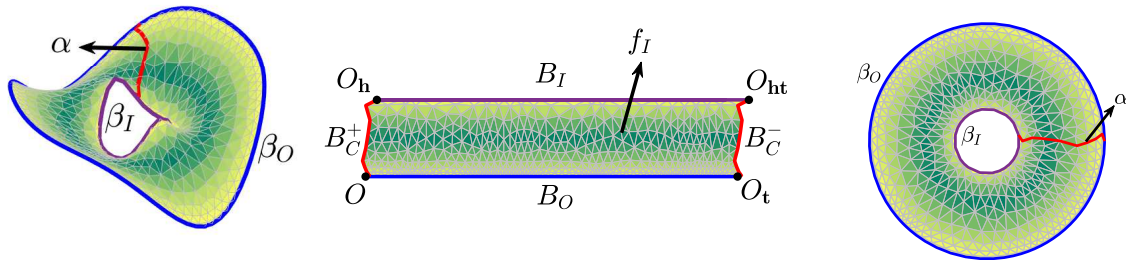
which can be conformally mapped to a poly-annulus, i.e., a unit disk with multiple circular holes.

Algorithm 1 Conformal parameterization for doubly connected surfaces by SPCF

Input: Double connected surface \mathcal{M} .

Output: An annulus conformal parameterization $f : \mathcal{M} \rightarrow \mathbb{C}$.

- 1: Find a path α from the outer boundary β_O to the inner boundary β_I .
 - 2: Cut the surface \mathcal{M} along the path α and obtain a single connected surface $\tilde{\mathcal{M}}$ with identical edges α^+, α^- .
 - 3: Build and solve the linear system $Ag = 0$ with $O = (0, 0)$, B_O on line $y = 0$ and B_I on line $y = 1$. Then construct the parameterized single periodic domain Ω by the solution.
 - 4: Impose the map (4.10) on Ω to obtain the target annulus.
-



(a) Double connected surface with slicing path α (b) Flattened single periodic quadrilateral band with straight boundaries (c) Annulus obtained by (4.10)

Figure 5: An illustrative example for conformal maps from double connected surface to a quadrilateral band and then to an annulus.

Inspired from [32, 4], for such a multiply connected genus-zero surface, we can select an inner boundary $\beta_\ell, \ell < N$ and fill the others to obtain a doubly connected surface, so that we can apply Algorithm 1 to compute the conformal map f_ℓ to transform the repaired surface to an annulus. Then select the next inner boundary and repeat the above operation. There exists the discrete distortions during this process and circles may become ellipses. Eventually \mathcal{M} can be mapped to a disk with multiple circular holes by a circular restriction and solving a Laplace-Beltrami equation, termed h . In this process, all the maps are conformal maps, so the final composite map $f := h \circ f_{N-1} \circ \dots \circ f_2 \circ f_1$ is also a conformal map. This approach is summarized as Algorithm 2.

Algorithm 2 Conformal parameterization for multiply connected surfaces by SPCF

Input: Multiply connected surface \mathcal{M} with N boundaries.

Output: A conformal parameterization $f : \mathcal{M} \rightarrow \mathbb{R}^2$.

- 1: Search all boundaries $\{\beta_\ell, \ell = 1, 2, \dots, N\}$. Set the longest boundary as the outer boundary β_N .
- 2: **for** $\ell = 1 : N - 1$ **do**
- 3: Fill the boundaries except β_ℓ .
- 4: Apply Algorithm 1 to transform \mathcal{M}_ℓ into an annulus $\hat{\mathcal{M}}_\ell$.
- 5: Remove the filled boundaries of $\hat{\mathcal{M}}_\ell$ and then obtain $\mathcal{M}_{\ell+1}$.
- 6: **end for**
- 7: Restrict the boundaries to be circles and fix the boundaries. Then compute interior vertices by solving the Laplace-Beltrami equation

$$L_{II}\mathbf{f}_I = -L_{IB}\mathbf{f}_B.$$

5 Numerical Experiments

In this section, we describe the numerical performance and phenomena of our proposed algorithms in various perspectives. All the experimental routines are executed in MATLAB R2024a on a personal computer with a 2.50GHz CPU and 64GB RAM. Most of the mesh models are taken from Thingi10K [33], poly-annulus-conformal-map (<https://github.com/garyptchoi/poly-annulus-conformal-map>) and Common 3D Test Models (<https://github.com/alecjacobson/common-3d-test-models>), some of which are remeshed properly. Some special meshes are manually generated by MATLAB built-in function *generateMesh* and proper deformations. The handle and tunnel loops are computed by ReebHanTun [8].

5.1 Double Periodic Conformal Flattening

The genus-one surface meshes for the experiment and their basic information are shown in the first row of Figure 6 and Table 1. The red and blue curves in Figure 6 represent the handle and tunnel loops computed by ReebHanTun [8]. In Table 1, # face and # vert. represent the number of triangle faces and vertices, respectively. δ and μ represent angle distortions and Beltrami coefficients, respectively, which measure the conformal accuracies of the resulting maps. We compare our results with Algorithm 1 in [31], which based on holomorphic differential theory. Surprisingly, we test more than 20 meshes and find that the conformal performance are mostly identical. There exists at most 0.2% relative errors between DPCF and Algorithm 1 in [31]. Hence, we only show the conformal accuracy of DPCF in Table 1. However, DPCF is almost 4 – 5 times more efficient. Additionally, Figure 6 shows the conformal distortion distributions of DPCF on 4 meshes. We can see that no additional conformal distortions occur near the cutting paths, showing the independent to the cutting paths of DPCF.

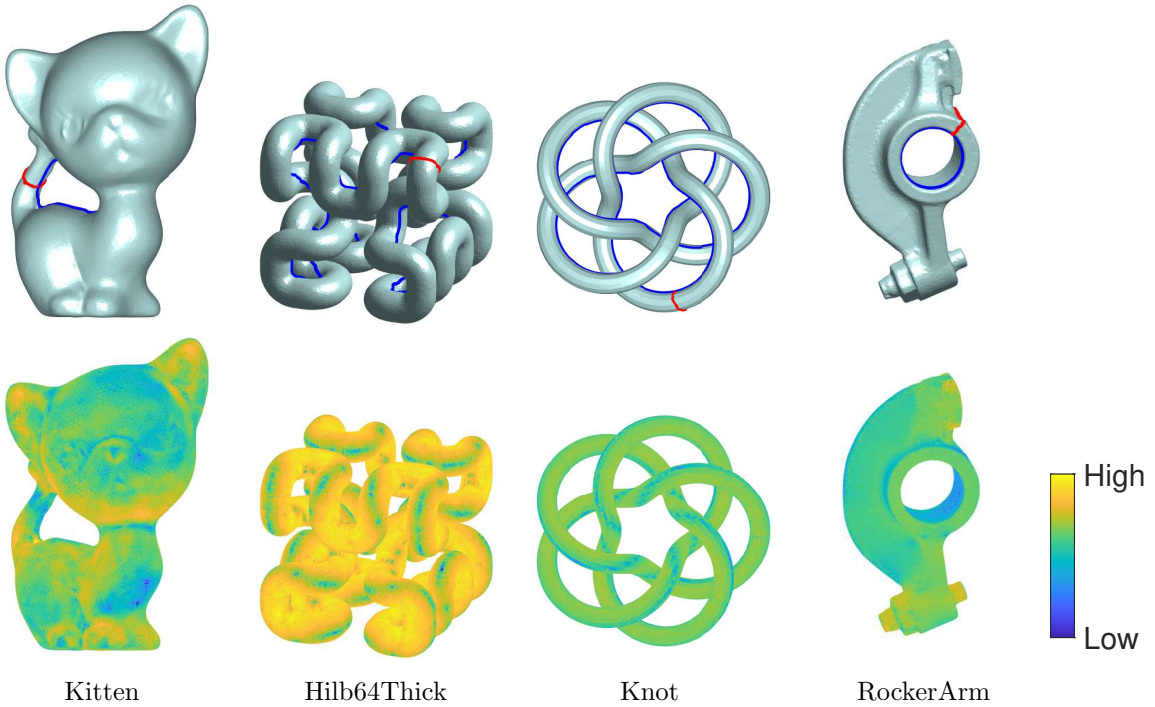


Figure 6: Genus-one mesh models for the double periodic flattening with handle and tunnel loops computed by ReebHanTun [8] and the angle distortion distributions of resulting maps by DPCF.

5.2 Single Periodic Conformal Flattening

Now, we show the performance of our proposed SPCF on doubly and multiply connected surfaces. We choose ACM (PACM) [4] for the comparison, whose code is obtained from <https://github.com/garyptchoi/poly-annulus-conformal-map>. The approach of ACM (PACM) is similar to Algorithm 1 and Algorithm 2, which tackles the holes one-by-one based on quasi-conformal theory. The another difference between ACM (PACM) and SPCF is that ACM (PACM)

Mesh	# face	# vert.	δ		$100 * \mu $		Time (s)		
			Mean	Std	Mean	Std	alg.1[31]	DPCF	ratio
Kitten	20000	10000	1.270	1.080	2.317	1.459	0.227	0.058	3.900
Hilb64Thick	64044	32022	1.249	0.929	2.000	1.000	0.894	0.161	5.544
Knot	169532	84766	0.248	0.230	0.393	0.298	2.782	0.539	5.158
RockerArm	309646	154823	0.275	0.385	0.438	0.517	4.761	0.894	5.324

Table 1: Comparison between Algorithm 1 in [31] and DPCF on genus-one surfaces. # face and # vert. represent the number of triangle faces and vertices, respectively.

transforms the cut mesh into a rectangle rather than a single periodic domain, the error on the cut path formed by which is tackled by the later quasi-conformal map on the annulus. In the PACM procedure, a optimal Möbius transformation is utilized to minimize the area distortion, which does not affect the conformal performance. Hence, we omit this step for the comparison.

The doubly and multiply connected surface meshes for the experiment and their basic information are shown in Figure 7 and Table 2. Table 2 also shows the performance in terms of accuracy and efficiency of ACM (PACM) and SPCF, in which ‘-’ means that the corresponding code does not work. It is seen that SPCF has much better performance in terms of efficiency and accuracy. Figure 8 depicts the cutting paths and angle distortion distributions of the resulting maps of ACM (PACM) and SPCF on the mesh *FlatTori* and *Alex*. The difference of holes on *Alex* is due to their different processing orders of holes. It is seen that ACM (PACM) leads to higher distortions near the cutting path, although a quasi-conformal map is utilized for the error occur on the cut path, while the angle distortion distribution of our proposed SPCF is independent to the cutting path.

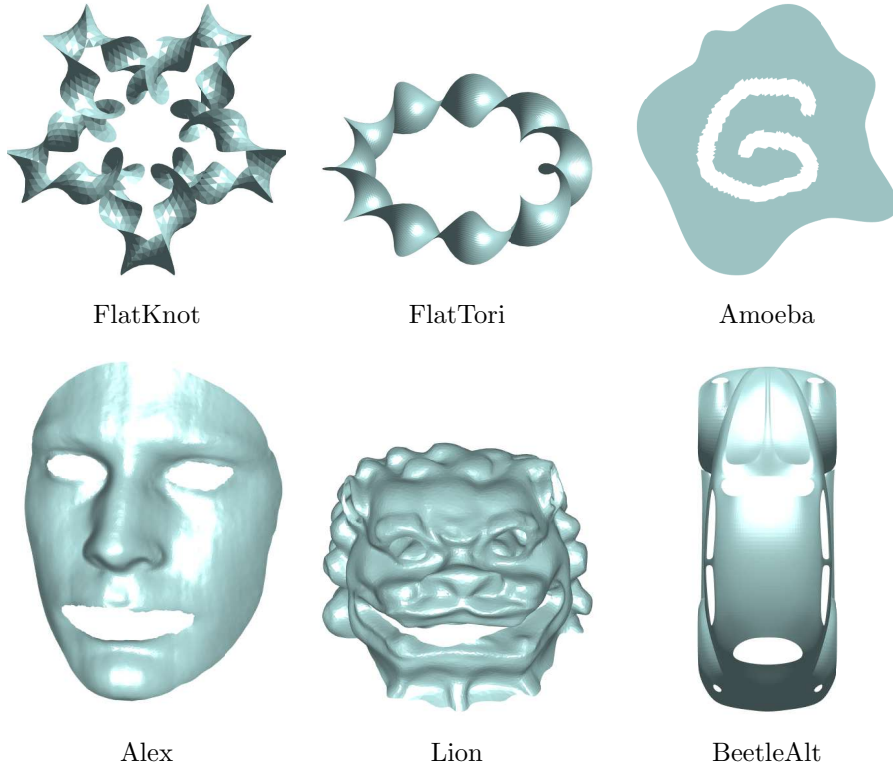


Figure 7: Doubly and multiply connected mesh models for annulus and poly-annulus conformal parameterizations.

Mesh	# face	# vert.	# bdry.	Alg.	δ		$100 * \mu $		Time (s)
					Mean	Std	Mean	Std	
FlatKnot	2800	1800	2	ACM [4]	4.020	4.767	6.625	7.314	0.061
				SPCF	3.150	2.426	5.347	2.502	0.020
FlatTori	11582	5917	2	ACM [4]	3.288	5.635	6.873	7.731	0.245
				SPCF	2.386	1.723	5.074	3.396	0.052
Amoeba	14045	7344	2	ACM [4]	4.013	7.018	6.839	9.333	0.266
				SPCF	3.642	7.829	6.464	10.65	0.077
Alex	37794	19280	4	PACM [4]	1.339	1.965	2.201	2.671	1.315
				SPCF	1.044	1.704	1.713	2.317	0.436
Lion	32819	16655	6	PACM [4]	6.769	6.857	11.183	8.737	1.661
				SPCF	2.746	3.336	4.548	4.409	0.458
BeetleAlt	38656	19887	11	PACM [4]	–	–	–	–	–
				SPCF	2.616	3.398	5.579	5.285	0.950

Table 2: Comparison between ACM (PACM) [4] and SPCF on doubly and multiply connected surfaces. # face and # vert. represent the number of triangle faces and vertices, respectively. # bdry. represents the number of the boundaries.

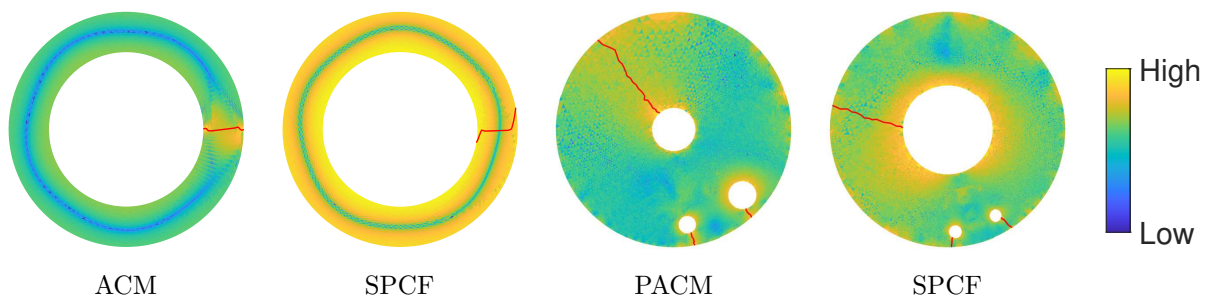


Figure 8: Angle distortion distributions of resulting maps by ACM (PACM) and SPCF on the mesh *FlatTori* and *Alex* with cut paths.

6 Conclusion

In this paper, we propose a novel periodic conformal flattening method for genus-one surfaces and multiply connected genus-zero surfaces. Similar to the seamless parameterization, the main advantage of our proposed method is that the computed conformal map is independent of the cut paths, and no additional bias occurs near the paths, which is suitable for applications in texture mapping and mesh generation. The periodic conformal flattening computation is based on the conformal energy minimization. For the surface flattening, the area term of the flattened polygon in the conformal energy can be expressed as a quadratic function with respect to the boundary vertices, and thus, even with the addition of the period condition, the discrete conformal energy is still a quadratic functional with respect to periods and vertices. Naturally, the conformal energy minimization problem is transformed into solving a linear system, which is the main reason for the high efficiency of our proposed algorithm. This property is then exploited to propose algorithms DPCF and SPCF for periodic conformal flattening for genus-one surface and doubly connected surface. And then the efficient annulus and poly-annulus parameterizations algorithms Algorithm 1 and Algorithm 2 are developed for doubly connected and multiply connected genus-zero surfaces based on the proposed SPCF. In the numerical experiments, we present the performance of DPCF and SPCF on genus-one surfaces and multiply connected genus-zero surfaces, respectively. The comparison with holomorphic approach [31] and ACM (PACM) [4] illustrates the low conformal distortion and almost 4-5 times of improvement in terms of efficiency. Additionally, the angle distortion distributions demonstrate the seamless property of our proposed algorithms.

In this paper, conformal energy shows its efficacy in surface flattening. However, the periodic flattening proposed herein depends on the topology of surfaces and the cutting paths, thus rendering it incompatible with arbitrary type of surfaces and cutting path patterns. For instance, higher-genus surfaces are not able to achieve such a translation-only flattening. The development of efficient seamless conformal flattening algorithms with higher generalisability by conformal energy minimization is one of our ongoing researches.

References

- [1] Noam Aigerman, Roi Poranne, and Yaron Lipman. Seamless surface mappings. 34(4), 2015.
- [2] Marcel Campen, Hanxiao Shen, Jiaran Zhou, and Denis Zorin. Seamless parametrization with arbitrary cones for arbitrary genus. 39(1), 2019.
- [3] Wei Chen, Siquan Sun, Yue Wang, Na Lei, Chander Sadasivan, Apostolos Tassiopoulos, Shikui Chen, Hang Si, and Xianfeng Gu. Robust surface remeshing based on conformal welding. In *Proceedings of the 2024 International Meshing Roundtable (IMR)*, pages 0–0, 2024.
- [4] Gary P. T. Choi. Efficient conformal parameterization of multiply-connected surfaces using quasi-conformal theory. *Journal of Scientific Computing*, 87(3), 2021.
- [5] Gary Pui-Tung Choi and Lok Ming Lui. A linear formulation for disk conformal parameterization of simply-connected open surfaces. *Advances in Computational Mathematics*, 44(1):87–114, 2018.
- [6] Pui Tung Choi and Lok Ming Lui. Fast disk conformal parameterization of simply-connected open surfaces. *Journal of Scientific Computing*, 65(3):1065–1090, 2015.
- [7] Mathieu Desbrun, Mark Meyer, and Pierre Alliez. Intrinsic parameterizations of surface meshes. *Computer Graphics Forum*, 21(3):209–218, 2002.
- [8] Tamal K. Dey, Fengtao Fan, and Yusu Wang. An efficient computation of handle and tunnel loops via reeb graphs. 32(4), 2013.
- [9] Qing Fang, Wenqing Ouyang, Mo Li, Ligang Liu, and Xiao-Ming Fu. Computing sparse cones with bounded distortion for conformal parameterizations. 40(6), 2021.
- [10] V.A. Garanzha, L.N. Kudryavtseva, and S.V. Utyuzhnikov. Variational method for untangling and optimization of spatial meshes. *Journal of Computational and Applied Mathematics*, 269:24–41, 2014.
- [11] Mark Gillespie, Boris Springborn, and Keenan Crane. Discrete conformal equivalence of polyhedral surfaces. *ACM Transactions on Graphics*, 40(4):1–20, 2021.

- [12] Xianfeng Gu and Shing-Tung Yau. *Computational Conformal Geometry*, volume 3 of *Advanced Lectures in Mathematics*. International Press and Higher Education Press, 2007.
- [13] Steven Haker, Sigurd Angenent, Allen Tannenbaum, Ron Kikinis, Guillermo Sapiro, and Michael Halle. Conformal surface parameterization for texture mapping. *IEEE Transactions on Visualization and Computer Graphics*, 6(2):181–189, 2000.
- [14] Kai Hormann and Günther Greiner. Mips: An efficient global parametrization method. *Curve and Surface Design: Saint-Malo 1999*, pages 153–162, 2000.
- [15] Wei-Qiang Huang, Xianfeng David Gu, Wen-Wei Lin, and Shing-Tung Yau. A novel symmetric skew-hamiltonian isotropic lanczos algorithm for spectral conformal parameterizations. *Journal of Scientific Computing*, 61(3):558–583, 2014.
- [16] John E. Hutchinson. Computing conformal maps and minimal surfaces. *Proceedings of the Centre for Mathematics and its Applications*, 26:140–161, 1991.
- [17] Miao Jin, Junho Kim, Feng Luo, and Xianfeng Gu. Discrete surface ricci flow. *IEEE Transactions on Visualization and Computer Graphics*, 14(5):1030–1043, 2008.
- [18] Liliya Kharevych, Boris Springborn, and Peter Schroeder. Discrete conformal mappings via circle patterns. *ACM Transactions on Graphics*, 25(2):412–438, 2006.
- [19] Yueh-Cheng Kuo, Wen-Wei Lin, Mei-Heng Yueh, and Shing-Tung Yau. Convergent conformal energy minimization for the computation of disk parameterizations. *SIAM Journal on Imaging Sciences*, 14(4):1790–1815, 2021.
- [20] U. Labsik, K. Hormann, and G. Greiner. Using most isometric parameterizations for remeshing polygonal surfaces. In *Proceedings Geometric Modeling and Processing 2000. Theory and Applications*, pages 220–228, 2000.
- [21] Bruno Lévy, Sylvain Petitjean, Nicolas Ray, and Jérôme Maillot. Least squares conformal maps for automatic texture atlas generation. *ACM Transactions on Graphics*, 21(3):362–371, 2002.
- [22] Mo Li, Qing Fang, Wenqing Ouyang, Ligang Liu, and Xiao-Ming Fu. Computing sparse integer-constrained cones for conformal parameterizations. 41(4), 2022.
- [23] Patrick Mullen, Yiyang Tong, Pierre Alliez, and Mathieu Desbrun. Spectral conformal parameterization. *Computer Graphics Forum*, 27(5):1487–1494, 2008.
- [24] Rohan Sawhney and Keenan Crane. Boundary first flattening. *ACM Transactions on Graphics*, 37(1):5:1–5:14, 2017.
- [25] Alla Sheffer and Eric de Sturler. Parameterization of faceted surfaces for meshing using angle-based flattening. *Engineering with Computers*, 17(3):326–337, 2001.
- [26] Alla Sheffer, Bruno Lévy, Maxim Mogilnitsky, and Alexander Bogomyakov. Abf++: Fast and robust angle based flattening. *ACM Transactions on Graphics*, 24(2):311–330, 2005.
- [27] Yousuf Soliman, Dejan Slepčev, and Keenan Crane. Optimal cone singularities for conformal flattening. *ACM Transactions on Graphics*, 37(4), 2018.
- [28] Jian-Ping Su, Chunyang Ye, Ligang Liu, and Xiao-Ming Fu. Efficient bijective parameterizations. *ACM Transactions on Graphics*, 39(4), 2020.
- [29] Qi Wang, Wen-Xiang Zhang, Yuan-Yuan Cheng, Ligang Liu, and Xiao-Ming Fu. Practical construction of globally injective parameterizations with positional constraints. *Computational Visual Media*, 9(2):265–277, 2023.
- [30] Yong-Liang Yang, Ren Guo, Feng Luo, Shi-Min Hu, and Xianfeng Gu. Generalized discrete ricci flow. *Computer Graphics Forum*, 28(7):2005–2014, 2009.
- [31] Mei-Heng Yueh, Tiexiang Li, Wen-Wei Lin, and Shing-Tung Yau. A new efficient algorithm for volume-preserving parameterizations of genus-one 3-manifolds. *SIAM Journal on Imaging Sciences*, 13(3):1536–1564, 2020.

- [32] Mei-Heng Yueh, Wen-Wei Lin, Chin-Tien Wu, and Shing-Tung Yau. An efficient energy minimization for conformal parameterizations. *Journal of Scientific Computing*, 73(1):203–227, 2017.
- [33] Qingnan Zhou and Alec Jacobson. Thingi10k: A dataset of 10,000 3d-printing models. *arXiv preprint arXiv:1605.04797*, 2016.